Photonic band structure of diamond colloidal crystals in a cholesteric liquid crystal

Setarehalsadat Changizrezaei*
Department of Physics and Astronomy, The University of Western Ontario, London, Ontario N6A 3K7, Canada.

Colin Denniston†
Department of Applied Mathematics, The University of Western Ontario, London, Ontario N6A 5B7, Canada. and Department of Physics and Astronomy, The University of Western Ontario, London, Ontario N6A 3K7, Canada.

(Dated: September 20, 2017)

In this paper, we demonstrate the presence of a photonic band gap for a diamond lattice structure made of particles with normal anchoring inside a cholesteric liquid crystal. As is typical for liquid crystals, there is considerable contrast between the dielectric constant parallel $\epsilon_\parallel$ and perpendicular $\epsilon_\perp$ to the director, with $\epsilon_\parallel/\epsilon_\perp \sim 4$ here. It is shown that the size of the photonic band gap is directly related to the size of colloidal particles and the contrast between the dielectric constant in the particles and the extreme values of ϵ in the LC medium (one needs either ϵ in the particle much smaller than $\epsilon_\perp$ *or* much bigger than $\epsilon_\parallel$). No opening is seen in the band diagrams for small particles. For larger particles a partial gap opens when the particles are composed of very low dielectric material, but never a complete gap. On the other hand, a complete gap starts to be revealed when the size of the colloidal particles is increased and when a high dielectric constant is used for filling inside the particles. The maximum size of the gap is observed when the particles are large enough so that their surfaces overlap.

PACS numbers: 61.30.Jf 47.57.J

I. INTRODUCTION

Periodic arrays of colloids can be viewed as periodic dielectric structures, and have been considered as prime candidates for photonic crystals [1–3]. Colloidal crystals are composed of particles of one material, such as silicon, inside a matrix made of another material, such as water. As these macroscopic media typically have differing dielectric constants, the result is a substance with a periodic dielectric function [4]. The periodicity in dielectric constant of a photonic crystal gives them the capability of controlling propagation of photons due to the refraction and reflection of light from different interfaces. In these structures, the light waves are similar to electron waves in atomic crystals. As a result, one of the possible features of photonic crystals is forbidding a certain range of frequencies to be propagated inside the periodic lattice. This feature makes a photonic crystal an ideal candidate to control, confine, and manipulate light propagation [4].

In 1990, it was demonstrated theoretically that a diamond lattice structure of spheres can show a complete band gap whereas an fcc lattice structure should not[5]. The kind of structure studied were spheres filled with air inside a dielectric medium. A practical face-centered-cubic dielectric structure with non-spherical "particles"and a complete gap was introduced in Ref. [6]. These sort of dielectric lattice structures have attracted considerable interest among researchers in the past decades [7–10].

One powerful and effective route to fabricate ordered colloidal particle structures is self-assembly of colloids in 2D and 3D in a fluid[11–15]. However, it is a challenge to generate a non-closed packed structure, which has the ability to show a complete band gap, meaning there is a forbidden range of frequencies for electromagnetic waves for all directions of wave propagations[4, 16]. The colloidal particles need to experience anisotropic forces in order to self-organize into such non-closed packed crystals. Therefore, a liquid crystal (LC) is potentially an ideal medium for the colloids to self-assemble in because it has unique anisotropic properties which result in colloidal particles experiencing anisotropic interactions. When the colloids are added into a LC medium, the particles are coupled to the director field orientation by specific orientational anchoring of LC molecules on the particle surface. As a result, the director is distorted from its uniform orientation close to the surface of particles. This director distortion generates topological defects close to the surface of particles [17]. The existence of defects inside the LC increases the elastic free energy [18, 19]. In order to minimize the elastic free energy, the distorted regions are shared between the particles, and anisotropic interactions are induced between them [20–23].

The preferred LC molecules orientation on the surface of colloidal particles, typically either tangential or normal, indicates the type of induced interactions. Here, we will use normal anchoring which can lead to two possible defect structures. The possible structure can be either a hyperbolic defect point [24], which is created near the surface of the particle and induces dipolar interaction between the colloids, or a Saturn-ring de-

*Electronic address: schangiz@uwo.ca
†Electronic address: cdennist@uwo.ca

fect line [25, 26] surrounding the colloid associated with quadropolar forces [17, 27]. It is seen that the Saturn-ring defect line is stable for small particles [28] like we use here.

In a LC medium, self-assembled structures are formed due to the induced forces between the particles at close ranges [29–32], where the regions of distortions are shared. A wide variety of colloidal structures have been observed [33–42]. In a cholesteric LC, the defect lines associated with colloidal inclusions are twisted depending on the value of the pitch [43, 44]. In Ref. [45] it is demonstrated that a locally stable diamond colloidal crystal can be obtained in a cholesteric. In this reference, several pitch values in a cholesteric LC were used in order to choose a pitch value generating the most energetically favorable diamond crystal built of colloids with normal surface anchoring. It was shown that the defect lines travel along the symmetry axis and a diamond crystal can be created. In addition, its stability was demonstrated by examining its phonon frequency spectrum.

The application to photonics is often cited as motivation for studying colloidal structures in liquid crystals but the photonic band structure that might be obtained has not been examined. It is known that there is a complete band gap in the band structure of a diamond crystal in an isotropic medium. In particular, it is known that the dielectric contrast between the dielectric constant inside the particles and the dielectric constant of the matrix is an important factor in determining whether a band gap occurs[4]. However, a LC medium is optically active due to its anisotropic nature and typically has a dielectric permeability that can change by a large factor depending on the direction of polarization relative to the liquid crystal's director field. As a result, it may change the band structure of such a colloidal diamond lattice. In this paper we analyze the photonic band structure of a diamond lattice made of colloidal particles immersed inside a cholesteric LC. The liquid crystal director is oriented normal to the particles surface and we selected the pitch value corresponding to the stable diamond structure found in Ref. [45].

II. MODELING

The hydrodynamics of a LC is mathematically described by considering a tensor order parameter **Q** based on the Landau-de Gennes theory [46]. The tensor order parameter has components defined as:

$$Q_{ij} = \langle \frac{3}{2}\hat{m_i}\hat{m_j} - \frac{1}{2}\delta_{ij} \rangle \,. \tag{1}$$

which depends on the direction of individual molecules $\hat{\mathbf{m}}$, and the angular brackets denote a coarse-grained average. **Q** is a symmetric traceless matrix. Its largest eigenvalue is $\frac{2}{3}q$ $(0 < q < 1)$, and shows the magnitude of order along the corresponding eigenvector, which defines the director field $\hat{\mathbf{n}}$.

The evolution of the tensor order parameter Q can be described by:

$$(\partial_t + \boldsymbol{u}\cdot\nabla)\boldsymbol{Q} - \boldsymbol{S}(\boldsymbol{W},\boldsymbol{Q}) = \Gamma \boldsymbol{H} \,. \tag{2}$$

Here, $\boldsymbol{S}(\boldsymbol{W},\boldsymbol{Q}) = (\xi\boldsymbol{D}+\Omega)(\boldsymbol{Q}+\boldsymbol{I}/3)+(\boldsymbol{Q}+\boldsymbol{I}/3)(\xi\boldsymbol{D}-\boldsymbol{\Omega})$ $-2\xi(\boldsymbol{Q}+\boldsymbol{I}/3)Tr(\boldsymbol{Q}\boldsymbol{W})$, where $\boldsymbol{D} = (\boldsymbol{W}+\boldsymbol{W}^T)/2$ and $\boldsymbol{\Omega} = (\boldsymbol{W}-\boldsymbol{W}^T)/2$ is related to the symmetric and anti-symmetric velocity gradient components $W_{\alpha\beta} = \partial_\beta u_\alpha$. ξ denotes the aspect ratio of LC molecules, and Γ is the collective rotational diffusion constant. Here, the primary purpose of the dynamics is just to take us to a minimum in the free energy. $\boldsymbol{H}$ is the functional derivative of the free energy of the system, ensuring the system evolves towards equilibrium and is given by:

$$\boldsymbol{H} = -\frac{\delta F}{\delta Q} + \left(\frac{\boldsymbol{I}}{3}\right)\frac{\delta F}{\delta Q} \,. \tag{3}$$

The Landau-de Gennes free energy is:

$$F_{bulk} = \frac{A_0}{2}(1-\frac{\gamma}{3})Q^2_{\alpha\beta} - \frac{A_0\gamma}{3}Q_{\alpha\beta}Q_{\beta\gamma}Q_{\gamma\alpha} + \frac{A_0\gamma}{4}\left(Q^2_{\alpha\beta}\right)^2 \,, \tag{4}$$

where $\gamma > 2.7$ yields a liquid crystalline phase, and A_0 is a constant. The distortion of the LC director field can be controlled by an elastic free energy:

$$\begin{aligned} F_{elastic} = \quad & \frac{L_1}{2}(\partial_\alpha Q_{\beta\gamma})^2 + \frac{L_2}{2}(\partial_\alpha Q_{\alpha\gamma})(\partial_\beta Q_{\beta\gamma}) \\ & + \frac{4\pi L_1}{P}\epsilon_{\alpha\beta\gamma}Q_{\alpha\nu}(\partial_\beta Q_{\gamma\nu}) \,, \end{aligned} \tag{5}$$

The distortion cost in a nematic LC is expressed through the first two terms and the last term is present to produce a helical pitch, P, in a cholesteric LC. The elastic constants L_1 and L_2 are easily mapped onto Frank elastic constants, K_1, K_2, K_3 [47].

Moreover, $F_{surface}$ is also present to model the interaction of the surface of colloidal particles with LC molecules. The applied surface boundary conditions and the anchoring strength α_s indicate the preferred orientation of LC director close to the surface of particles. We only use normal boundary conditions on the surface of spherical colloids here, which is dictated by:

$$F_{surface} = \frac{\alpha_s}{2}(Q_{ij} - Q^0_{ij})^2 \,, \tag{6}$$

where $Q^0_{ij} = q^0(\hat{n_i}^0\hat{n_j}^0 - \frac{1}{3}\delta_{ij})$, $\hat{\mathbf{n}}^0$ is the normal to the particles' surface, and q^0 is the the equilibrium bulk value of q. Like all fluids, the LC also satisfies Navier-Stokes and continuity equations.

It this paper, we work primarily near the minimum found for the diamond colloidal crystal in the cholesteric found in Ref. [45]. As such, we just use the dynamics to take us to this already established stable minima. As such, the colloidal particles are placed in the previously found location and the configuration of the liquid crystal is then minimized around that. As such, the colloids

are held fixed in all simulations (in equilibrium the forces in this configuration are all zero, as previously found in Ref. [45]). All the above equations are mathematically modeled using a lattice Boltzmann algorithm on a uniform mesh [48–50]. The surface of the colloids are discretized into a set of nodes (6252 nodes), and are interpolated onto the LC grid to the nearest LC lattice sites, so the forces and the fluid stresses can be calculated. It is worth mentioning that the algorithm is mainly used for evolving through the steady state and it was implemented inside LAMMPS [51]. The details about how this method is implemented are described in references [52–56].

A liquid crystal has an anisotropic dielectric constant which is different along and perpendicular to the director. The LC dielectric is dependent on the tensor order parameter as follows [46]:

$$\epsilon_{\alpha\beta} = \frac{2}{3}\epsilon_a Q_{\alpha\beta} + \epsilon_m \delta_{\alpha\beta}\,, \tag{7}$$

where

$$\begin{aligned} \epsilon_a &= \frac{3}{2q}\left(\epsilon_\parallel - \epsilon_\perp\right)\,, \\ \epsilon_m &= \frac{2}{3}\epsilon_\perp + \frac{1}{3}\epsilon_\parallel\,. \end{aligned} \tag{8}$$

$\epsilon_\parallel$ and $\epsilon_\perp$ are the relative permittivity along and perpendicular to the director. The values used are shown in table I and are typical of readily available liquid crystals. Note that the ratio $\epsilon_\parallel/\epsilon_\perp \approx 4$ is comparable or larger than the typical dielectric contrast of, say, previously studied systems of a diamond lattice of dielectric spheres in air [4](where the contrast is usually between the sphere contents and the surrounding matrix, whereas in our case this will be a variation within the matrix surrounding the spheres). This is why we cannot just assume that the band structures seen using a matrix with an isotropic dielectric constant will be comparable to what we will find here.

In this paper, photonic band structures of periodic dielectric spherical particles in a diamond lattice structure are calculated using Maxwell equations through the MIT Photonic-Bands (MPB) package. The package was modified slightly to take ϵ input from the order parameter and colloids obtained from the lattice Boltzmann simulations but was otherwise used as given. Similar to the assumptions mentioned in reference [4], the dielectric material is assumed to be only dependent on the position $\boldsymbol{r}$, and the value of charge and current density are set to be zero as there are not any light sources. Another assumption is that the electric displacement $\boldsymbol{D}$ and electric field $\boldsymbol{E}$ are linearly proportional to each other as follows:

$$D_\alpha(r) = \epsilon_0 \epsilon_{\alpha\beta}(r) E_\beta(r)\,, \tag{9}$$

where $\boldsymbol{\epsilon}(\boldsymbol{r})$ is the tensor dielectric function. There is also linear proportionality between the magnetic field $\boldsymbol{H}(\boldsymbol{r})$ and the magnetic induction field $\boldsymbol{B}(\boldsymbol{r})$ as given by:

$$B_\alpha(r) = \mu_0 \mu_{\alpha\beta}(r)) H_\beta(r) \approx \mu_0 H_\beta(r)\,, \tag{10}$$

TABLE I: Simulation parameters

Symbol	Value	Units
A_0	0.5	atm
γ	3.103	—
K_1	15	pN
K_2	6.7	pN
K_3	15	pN
Γ	0.33775	$atm^{-1}.\mu m^{-1}$
ξ	0.52	—
Δx	0.0625	μm
Δt	0.5	μs
P_0	1.0	atm
$\epsilon_\parallel$	19.0	—
$\epsilon_\perp$	5.2	—
a	5.5	μm

where the magnetic permeability $\boldsymbol{\mu}(\boldsymbol{r})$ is close to unity so we will ignore its tensor nature and spatial variation (The diamagnetic susceptibility, $1-\mu$ of liquid crystals is very small, typically around 10^{-6} [57]). Moreover, the dielectric tensor $\boldsymbol{\epsilon}(\boldsymbol{r})$ is a real, and positive definite tensor based on its dependence on $\mathbf{Q}$ in Eq.(7).

In the MPB program, the following harmonic modes are used for electric and magnetic fields as the Maxwell equations are linear and the temporal and spatial dependence can be separated. So the fields are given as:

$$\begin{aligned} \boldsymbol{H}(\boldsymbol{r},t) &= \boldsymbol{H}(\boldsymbol{r}) e^{-i\omega t} \\ \boldsymbol{E}(\boldsymbol{r},t) &= \boldsymbol{E}(\boldsymbol{r}) e^{-i\omega t} \end{aligned} \tag{11}$$

The transversality condition can be determined by considering the following divergence equation:

$$\begin{aligned} \partial_\alpha H_\alpha(r) &= 0 \\ \partial_\alpha \epsilon_{\alpha\beta}(r) E_\beta(r) &= 0 \end{aligned} \tag{12}$$

Furthermore, we have the following curl equations for electric and magnetic fields:

$$\begin{aligned} \varepsilon_{\alpha\beta\gamma}\partial_\beta E_\gamma - i\omega\mu_0 H_\alpha(r) &= 0 \\ \varepsilon_{\alpha\beta\gamma}\partial_\beta H_\gamma + i\omega\epsilon_0\epsilon_{\alpha\beta}(r) E_\beta(r) &= 0 \end{aligned} \tag{13}$$

where $\varepsilon_{\alpha\beta\gamma}$ is the Levi-Civita tensor ($\varepsilon_{\alpha\beta\gamma}\partial_\beta E_\gamma$ is the α component of $\nabla \times \mathbf{E}$). The above equations can be written to obtain a master equation depending only on $\boldsymbol{H}(\boldsymbol{r})$ as follows:

$$\varepsilon_{\alpha\beta\gamma}\partial_\beta \left[\epsilon^{-1}_{\gamma\eta}(r)\varepsilon_{\eta\mu\nu}\partial_\mu H_\nu(r)\right] = \left(\frac{\omega}{c}\right)^2 H_\alpha(r) \tag{14}$$

where ϵ^{-1} is the matrix inverse of ϵ, and c is the speed of light.

We can use the master equation to obtain the frequencies corresponding to each states $\boldsymbol{H}(\boldsymbol{r})$ for a defined dielectric function. Using Bloch's theorem, we can consider $\boldsymbol{H}(\boldsymbol{r})$ as a plane wave:

$$\boldsymbol{H}(\boldsymbol{r}) = e^{ik\cdot r}\boldsymbol{u}(\boldsymbol{r}) \tag{15}$$

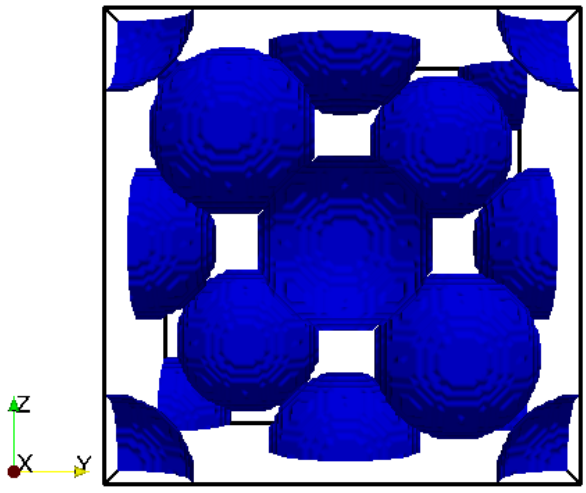

a)

FIG. 1: High, $\epsilon = 70$, contour of ϵ for the particles of radius $17\Delta x$ ($\sim$1.1 μm). The blue contour shows the regions inside of which ϵ is isotropic and its value is set to 70. The liquid crystal, with anisotropic ϵ, given by Eq. 7, fills the space outside this contour.

$\boldsymbol{u}(\boldsymbol{r})$ and $\boldsymbol{\epsilon}(\boldsymbol{r})$ can be expanded as Fourier series as they are periodic functions on the lattice:

$$\begin{aligned} \boldsymbol{u}_{\boldsymbol{k}}(\boldsymbol{r}) &= \sum_G \boldsymbol{c}_{\boldsymbol{G}}(\boldsymbol{k}) e^{i\boldsymbol{G}\cdot r} \\ \boldsymbol{\epsilon}_{\boldsymbol{k}}(\boldsymbol{r}) &= \sum_G \boldsymbol{c}_{\boldsymbol{G}}(\boldsymbol{k}) e^{i\boldsymbol{G}\cdot r}\,, \end{aligned} \tag{16}$$

where $\boldsymbol{G}$ is reciprocal lattice vector ($\boldsymbol{G}\cdot\boldsymbol{R} = 2\pi n$). As a result, the master equation can be solved as an eigenvalue problem in which $\left(\frac{\omega}{c}\right)^2$ is the eigenvalues corresponding to each discrete harmonic modes. Further details can be found in reference [4].

III. RESULTS

In our work, different diamond lattices constructed from 8 particles were considered inside a cholesteric LC. In reference [45], it was found that the most energetically favorable stable colloid diamond crystal can be formed in a cholesteric LC with pitch value equal to the lattice constant a. Therefore, we use the same pitch value. The simulation box is periodic in x, y, and z directions, and its dimensions is $(88 \times 88 \times 88)\Delta x$, which is commensurate with the chosen pitch value (5.5 μm). The applied boundary condition for the director on the surface of each of these 8 spherical colloids is perpendicular. As a result, Saturn-ring like defects are created around each of them when located in a nematic LC, but the rings are twisted around the particles when they are inside a cholesteric LC [44].

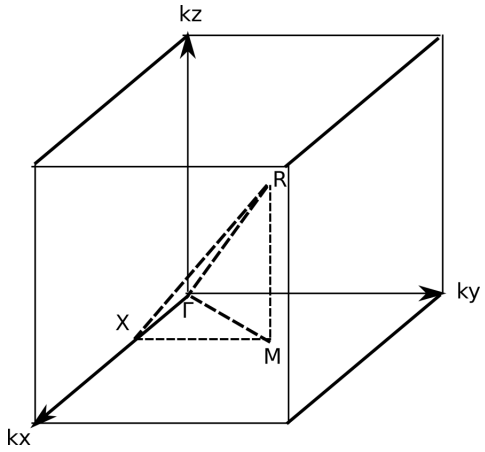

FIG. 2: Irreducible Brillouin zone for the simple cubic lattice.

In ref. [45], different initial states were used in order to investigate the effect of the initialization of the cholesteric LC on the possible defect structures formed in the colloidal diamond lattice. We used the configuration leading to the lowest free energy that was found in Ref. [45]. For the case where the matrix is isotropic it was found that varying the particle size relative to the lattice constant had a very significant effect on the size of the band gap [4]. Here we use a few different particles sizes and assume that the low energy structure and stability is similar to that found in [45] for the particles of radius $17\Delta x$ ($\sim$1.1 μm). This is probably not true for the smallest diameter spheres ($10\Delta x$) studied here, as the resulting defect structure ends up noticeably different from that found for the $17\Delta x$ case. However, we shall see that the smaller particles do not have a band gap so it is probably not worthwhile studying the stability of that case further. The defect structure for the larger spheres were all very similar so they should have comparable stability properties to the case studied in [45].

In order to generate the periodic dielectric lattice structure, the dielectric tensor outside the spheres is set using Eq. (7) and inside the colloidal particles an isotropic dielectric tensor is set as follows:

$$\begin{bmatrix} \epsilon & 0 & 0 \\ 0 & \epsilon & 0 \\ 0 & 0 & \epsilon \end{bmatrix}, \tag{17}$$

where ϵ is the interior dielectric constant. We chose a range of values between low ($\epsilon = 1$), and high ($\epsilon = 70$) dielectric constant value for the isotropic dielectric inside each particle to get a high dielectric contrast with the LC medium. The contour of isotropic ϵ can be seen in figure 1 for one such case.

In order to study the photonic bands, a simple cubic irreducible Brillouin zone with its corresponding reciprocal lattice points is considered which is shown in figure 2. This figure illustrates the path on the edge of the Brillouin zone, labeled by points Γ, X, R, M corresponding to different wave-vectors. We chose the points Γ, X, M,

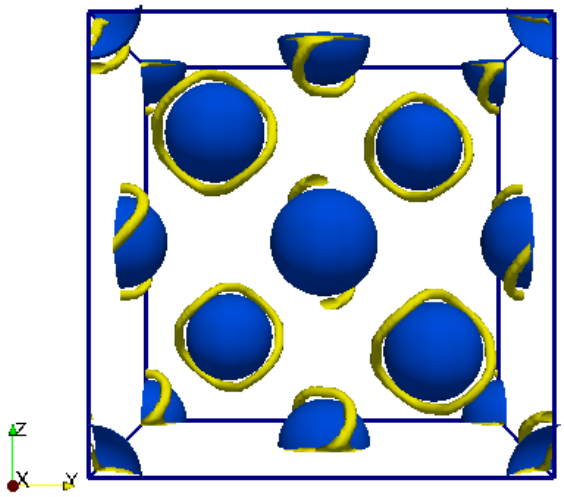

FIG. 3: The diamond lattice made of colloids with radius $10\Delta x$ with a (yellow) contour of the scalar order parameter (14% below the bulk value) showing the Saturn-ring-like defects surrounding each colloid.

R with 4 interpolated points in between of each point along the path Γ X M R, and calculated the eigenvalues of Eq. (14) using the MPB package and plotted the band diagrams for the lattice.

First, we start with small particles of radius $10\Delta x$ (0.625 μm) as shown in Figure 3. In this figure, representing the equilibrated state of the liquid crystal (i.e. the liquid crystal was evolved to the steady state), the yellow tube-like lines indicate the location of disclination lines surrounding the colloids. They show a contour of the locations where the scalar order parameters (largest eigenvalue of $\mathbf{Q}$) drops about 14% from its bulk value. In this case, the surface separations between the closest particles is about $18\Delta x$; therefore, the particles are far from each other and the defect lines do not join each other.

The dielectric constant inside the sphere is set to $\epsilon = 1$ and then the band structure is evaluated from a corresponding set of 20 eigenvalues at the edge of the Brillouin zone. Figure 4(a) demonstrates that no band gap is seen in this case and some of the frequencies are degenerate in the photonic band structure. We then set the dielectric constant inside the sphere to a higher value ($\epsilon = 70$) and repeat the band structure calculation. Again, as seen in Fig. 4(b), there is also no gap seen in the band diagrams. This example is somewhat of the extreme case and so the result is perhaps not that surprising given that an isotropic matrix with such small colloidal inclusions organized into a diamond crystal would not be expected to have a band gap either [4]. However, given that our LC matrix has a dielectric permeability that varies by nearly a factor of four ($\epsilon_\perp$ versus $\epsilon_\parallel$) it is not necessarily expected to behave in the same way as an isotropic matrix.

Next, we examined the eigenvalues at reciprocal lattice points when the particle radius is increased to $17\Delta x$

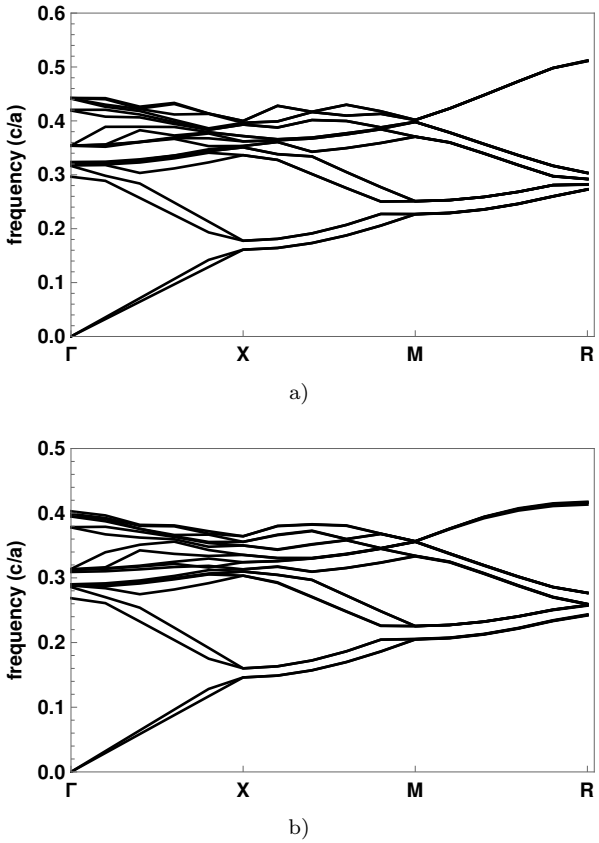

FIG. 4: The photonic band structures for particles of radius $10\Delta x$ filled with a) $\epsilon = 1$, and b) $\epsilon = 70$.

(~ 1.1 μm). This situation is identical to the one studied in Ref. [45] where it was established that it was a stable minimum of the free energy. In this case, the closest particle separation is now $4\Delta x$, and the defect lines are joined to each other and travel along symmetry lines of the lattice, which is shown in Figure 5. The photonic band structure is shown in Figure 6 for three different values of the dielectric constant inside the spheres. When the lowest dielectric constant ($\epsilon = 1$) is used in the sphere, no gap is seen in the photonic band diagram. When the particle's dielectric constant is increased to ($\epsilon = 48$) a narrow partial gap opens in the band diagram (we also checked $\epsilon = 45$ and found the bands just touching). When the higher dielectric constant ($\epsilon = 70$) is used, we see that bands open partially which means we must tunnel through the bands to control the propagation of specific chosen frequencies. Also, when $\epsilon = 70$ the range of calculated frequencies narrows compared to the lower values.

When the radius of particles is increased to $19\Delta x$, the closest neighbor particle's surfaces touch each other. The contour of the maximum eigenvalue of tensor order parameter is shown in Figure 7 where it dips below the bulk value, indicating the presence of a disclination. This figure illustrates that when the particles get too close to each other a second small "defect" ring appears where

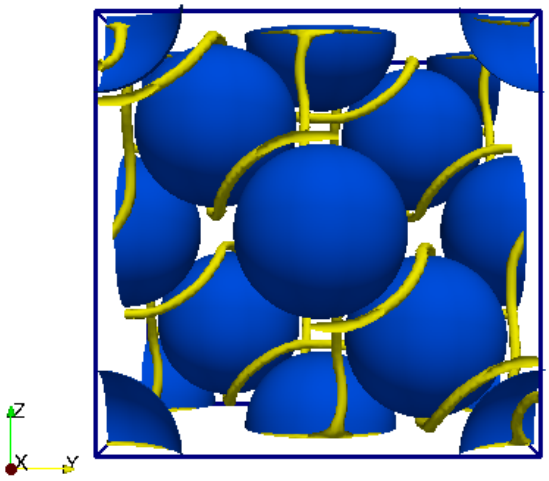

FIG. 5: The diamond lattice made of colloids with radius $17\Delta x$ with a (yellow) contour of the scalar order parameter showing the disclination lines traveling along symmetry lines of the lattice.

the colloids meet (the sphere in the front-center is drawn transparently in order to make this visible). This is probably related to the slight mismatch of the surface directors on the two colloids as one moves away from the exact point of contact and is not a true disclination, just a softening of the local order to avoid a "kink"in the director field.

The band structure for different ϵ values for the particle interior is shown in Figure 8. At the lowest value of $\epsilon = 1$, as seen in Fig. 8(a), there is now a slight partial gap, something not seen for the smaller spheres. This partial gap disappears when ϵ is increased, as seen in the results for $\epsilon = 2.31$ (Fig. 8b). As ϵ is increased further a partial gap reopens near $\epsilon \approx 40$. Increasing ϵ inside the spheres further still, when $\epsilon = 70$, Figure 8c demonstrates that there is now a complete, but narrow, gap between band 8 and 9, and its size is about 4.2%. The size of the gap is identified through the gap-midgap ratio, defined as the ratio of $\Delta\omega/\omega_m$, where $\Delta\omega$ is the frequency width of photonic band gap, and ω_m is the frequency at the middle of the gap [4].

Finally, we evaluate the photonic band diagram for slightly larger colloidal particles, so that they overlap each other. This can be practically done by making the spheres out of elastic material and compressing the system slightly. The resulting band structure is shown in Fig. III. At a particle radius of $20\Delta x$, the size of the gap in band structure increases to 6.3% when the higher dielectric constant is used ($\epsilon = 70$). When ϵ is set to it's lowest value ($\epsilon = 1$), a partial gap appears in the photonic bands which must be tunneled through the corresponding frequencies to prevent light propagation for the specific frequency range. Though there is a larger partial gap at $\epsilon = 1$ than was seen for the particles of radius $19\Delta x$, this partial gap again disappears when ϵ is increased to 2.31. So, overall, the onset of the appearance

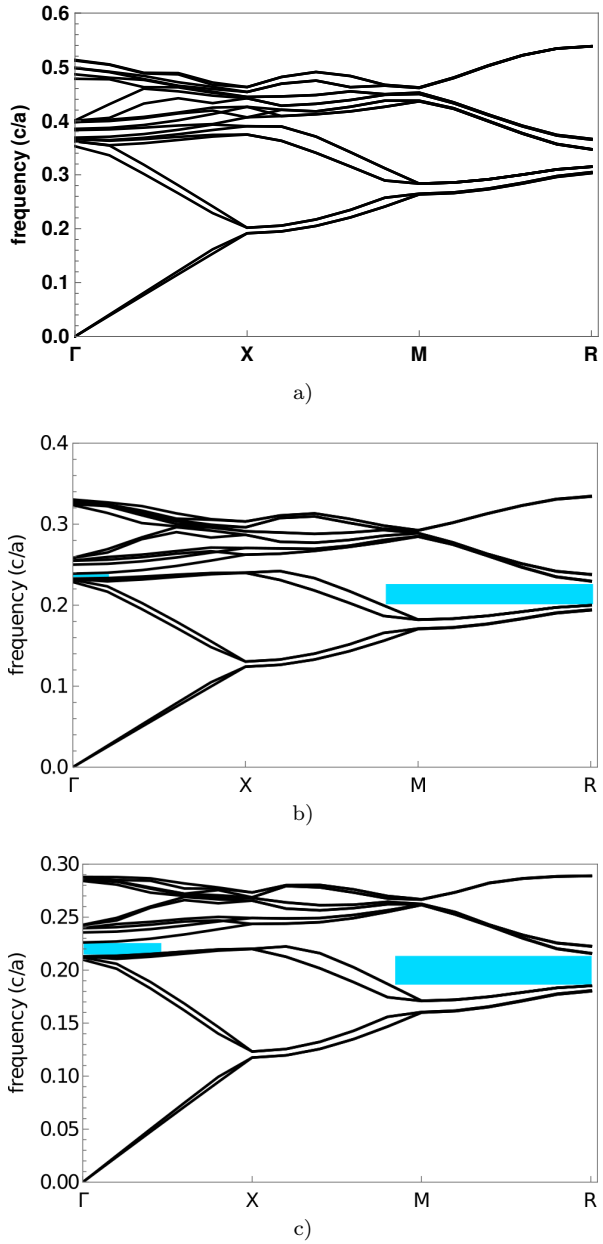

FIG. 6: The photonic band structures for particles of radius $17\Delta x$ filled with a) $\epsilon = 1$, b) $\epsilon = 48$, and c) $\epsilon = 70$.

of the (partial) gaps is similar to the $19\Delta x$ spheres, but the gaps grows slightly faster as the dielectric constant of the sphere moves away from these onset points.

These sort of photonic band diagram examinations illustrate that using spheres in a cholesteric liquid crystal is a promising method to build non-closed packed colloidal lattices with a desirable photonic band gap by adjusting two important factors: particle size and proper dielectric constant of the sphere to generate appropriate dielectric contrast ratio with the LC medium.

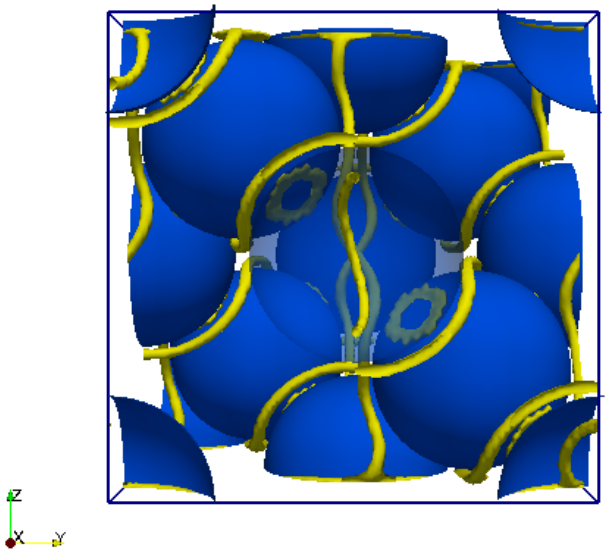

FIG. 7: The diamond lattice made of colloids with radius $19\Delta x$ with the contour plot of scalar order parameter showing the line defects surrounding each colloid. The front-center sphere is drawn transparently so that the circular distortion where the spheres meet is visible.

IV. DISCUSSION AND CONCLUSIONS

In Ref.[45] it was demonstrated that a diamond colloidal crystal could be stable in a cholesteric liquid crystal. Here, we have demonstrated the dielectric properties of the colloids that would be necessary for such a crystal to exhibit a photonic band gap. We demonstrate that the photonic response of the diamond array of colloids inside a LC depends on two main features: the dielectric constant of colloids inside the LC, and the size of colloids.

We considered Maxwell equations and used Bloch's theorem assuming the magnetic field as a plane wave, and a Fourier series expansion for periodic functions on the lattice such as the dielectric function($\epsilon_k(r)$), and the periodic function used for magnetic function($u_k(r)$). We calculated the frequencies for 20 bands at the edge of the SC irreducible BZ to explore the photonic band structure for the diamond colloidal crystal immersed in LC.

Comparing the band diagrams for different particle sizes and the dielectric constants of colloids, it was found that small spherical particles ($r = 10\Delta x$) do not show any gaps in the photonic band structures and the bands cross each other at some reciprocal lattice points on the edge of Brillouin zone. There is no opening in the band diagram for small particles at the low or high dielectric constants used for colloids.

The photonic band structures reveal different results for larger colloids. When the particles with $r = 17\Delta x$ and a higher dielectric constant are used in the diamond array inside the LC, we see a partial band gap across the reciprocal lattice points, meaning there is a local frequency range in which the light wave cannot be propagated. On the other hand, no local opening is seen in the band diagram when the lower dielectric constant value is used and there is degenerate frequencies at some points.

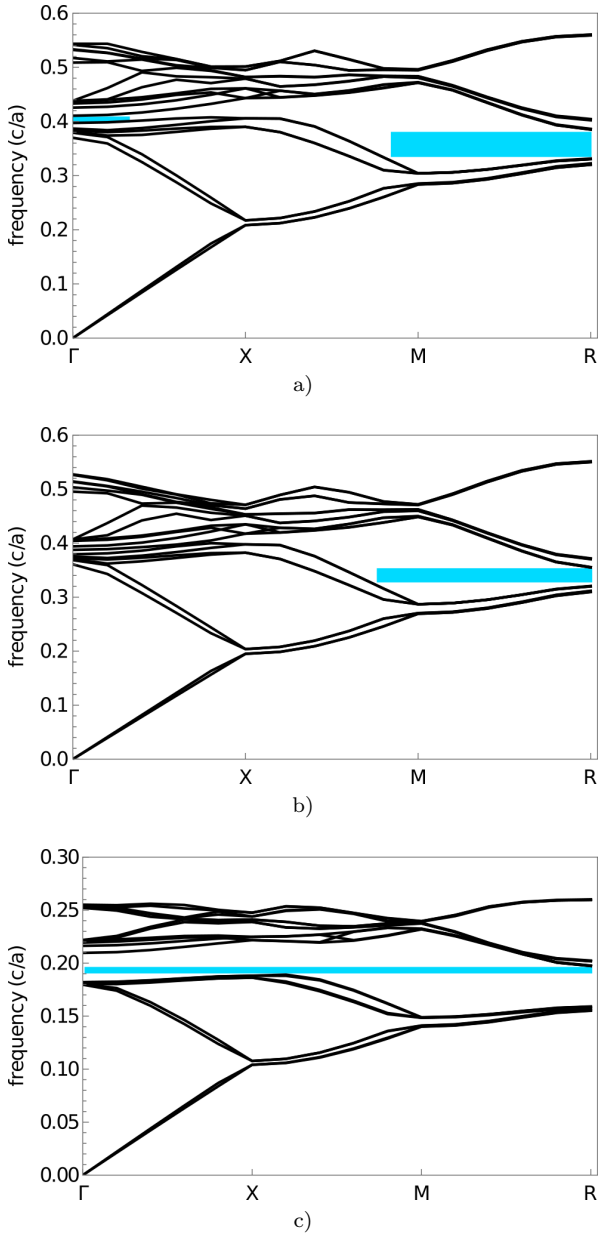

FIG. 8: The photonic band structures for particles of radius $19\Delta x$ filled with a) $\epsilon = 1$, a) $\epsilon = 2.31$, and b) $\epsilon = 70$.

Even more interesting results are explored when even larger particles are used to form a diamond crystal. When the particles are large enough in order for their surfaces to touch each other, a narrow complete band gap with size 4.2% appears at the highest dielectric contrast. There is a small partial gap at the lowest ϵ, but no complete gap. A larger complete band gap is observed when the size of colloids are larger so the particle's surfaces overlap. Therefore, our work offers a means to produce the desired photonic diamond colloidal crys-

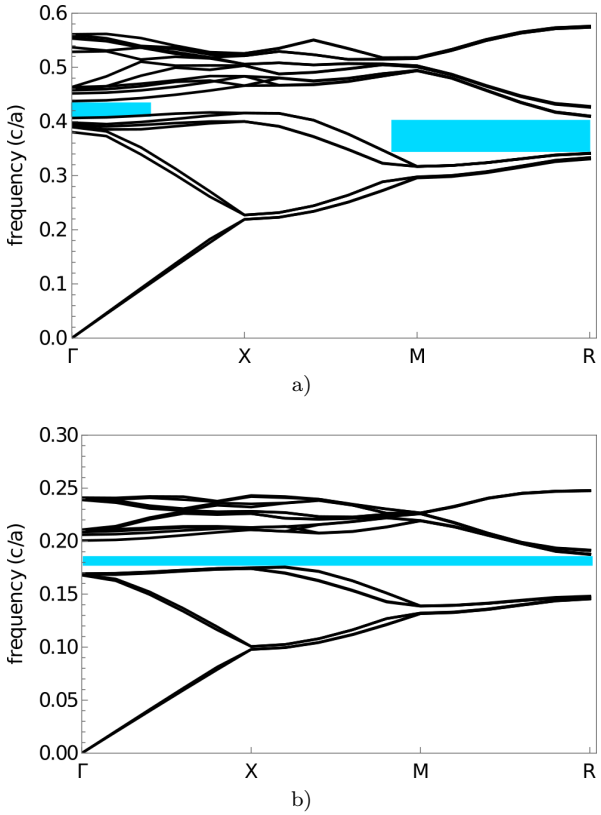

FIG. 9: The photonic band structures for particles of radius $20\Delta x$ filled with a) $\epsilon = 1$, and b) $\epsilon = 70$.

tals with different complete band gaps sizes, which have useful applications in photonics. The optimum particle size (preferably large particles) with high dielectric ratio contrast in the medium reveal a complete band gap.

Acknowledgments

We would like to thank the Natural Science and Engineering Research Council of Canada (NSERC) for financial support. This research has been enabled by the use of computing resources provided by Shared Hierarchical Academic Research Computing Network (SHARCNET) and Compute/Calcul Canada.

[1] V. L. Colvin, MRS Bulletin **26**, 637641 (2001).
[2] J. Ge, Y. Hu, and Y. Yin, Angewandte Chemie International Edition **46**, 7428 (2007), ISSN 1521-3773, URL http://dx.doi.org/10.1002/anie.200701992.
[3] Y. Fang, B. M. Phillips, K. Askar, B. Choi, P. Jiang, and B. Jiang, J. Mater. Chem. C **1**, 6031 (2013), URL http://dx.doi.org/10.1039/C3TC30740A.
[4] J. Joannopoulos, S. Johnson, J. Winn, and R. Meade, *Photonic Crystals: Molding the Flow of Light, 2nd ed.* (Princeton University Press, 2008).
[5] K. M. Ho, C. T. Chan, and C. M. Soukoulis, Phys. Rev. Lett. **65**, 3152 (1990), URL http://link.aps.org/doi/10.1103/PhysRevLett.65.3152.
[6] E. Yablonovitch, T. J. Gmitter, and K. M. Leung, Phys. Rev. Lett. **67**, 2295 (1991), URL http://link.aps.org/doi/10.1103/PhysRevLett.67.2295.
[7] NoritsuguYamamoto, SusumuNoda, and AlongkarnChutinan, Japanese Journal of Applied Physics **37**, L1052 (1998), URL http://stacks.iop.org/1347-4065/37/i=9A/a=L1052.
[8] KuonInoue, MichihideSasada, JunKawamata, KazuakiSakoda, and J. W.Haus, Japanese Journal of Applied Physics **38**, L157 (1999), URL http://stacks.iop.org/1347-4065/38/i=2B/a=L157.
[9] T. Baba, Nature Photonics **2**, 465 (2008).
[10] E. Ozbay, I. Bulu, K. Aydin, H. Caglayan, and K. Guven, Photonics and Nanostructures - Fundamentals and Applications **2**, 87 (2004), ISSN 1569-4410, URL http://www.sciencedirect.com/science/article/pii/S1569441004000422.
[11] S. Im, Y. Lim, D. Suh, and O. O. Park, Advanced Materials **14**, 1367 (2002), ISSN 1521-4095, URL http://dx.doi.org/10.1002/1521-4095(20021002)14:19<1367::AID-ADMA1367>3.0.CO;2-U.
[12] F. Garca-Santamara, V. Salgueirio-Maceira, C. Lpez, and L. M. Liz-Marzn, Langmuir **18**, 4519 (2002), http://dx.doi.org/10.1021/la025594t, URL http://dx.doi.org/10.1021/la025594t.
[13] J. Zhang, Y. Li, X. Zhang, and B. Yang, Advanced Materials **22**, 4249 (2010), ISSN 1521-4095, URL http://dx.doi.org/10.1002/adma.201000755.
[14] A. K. Boal, F. Ilhan, J. E. DeRouchey, T. Thurn-Albrecht, T. P. Russell, and V. M. Rotello, Nature **404**, 746 (2000).
[15] B. Gates, S. H. Park, and Y. Xia, Proc. SPIE **3937**, 36 (2000), URL http://dx.doi.org/10.1117/12.382812.
[16] M. Florescu, S. Torquato, and P. J. Steinhardt, Phys. Rev. B **80**, 155112 (2009), URL http://link.aps.org/doi/10.1103/PhysRevB.80.155112.
[17] P. Poulin and D. A. Weitz, Phys. Rev. E **57**, 626 (1998).
[18] H. Stark, Physics Reports **351**, 387 (2001), ISSN 0370-1573.
[19] M. Tasinkevych, N. M. Silvestre, and M. M. T. da Gama, New Journal of Physics **14**, 073030 (2012).

[20] F. E. Mackay and C. Denniston, Soft Matter **9**, 5285 (2013).

[21] J. S. Lintuvuori, K. Stratford, M. E. Cates, and D. Marenduzzo, Phys. Rev. Lett. **107**, 267802 (2011), URL https://link.aps.org/doi/10.1103/PhysRevLett.107.267802.

[22] O. Guzmán, E. B. Kim, S. Grollau, N. L. Abbott, and J. J. de Pablo, Phys. Rev. Lett. **91**, 235507 (2003).

[23] M. R. Mozaffari, M. Babadi, J.-i. Fukuda, and M. R. Ejtehadi, Soft Matter **7**, 1107 (2011).

[24] M. Kleman and O. D. Lavrentovich, Philosophical Magazine **86**, 4117 (2006).

[25] T. C. Lubensky, D. Pettey, N. Currier, and H. Stark, Phys. Rev. E **57**, 610 (1998).

[26] O. V. Kuksenok, R. W. Ruhwandl, S. V. Shiyanovskii, and E. M. Terentjev, Phys. Rev. E **54**, 5198 (1996).

[27] I. Musevic, M. Skarabot, U. Tkalec, M. Ravnik, and S. Zumer, Science **313**, 954 (2006), ISSN 00368075, 10959203, URL http://www.jstor.org/stable/3846976.

[28] H. Stark, Physics Reports **351**, 387 (2001), ISSN 0370-1573.

[29] P. Poulin, H. Stark, T. C. Lubensky, and D. A. Weitz, Science **275**, 1770 (1997), ISSN 0036-8075, http://science.sciencemag.org/content/275/5307/1770.full.pdf, URL http://science.sciencemag.org/content/275/5307/1770.

[30] J.-C. Loudet, P. Barois, and P. Poulin, Nature **407**, 611 (2000).

[31] M. Yada, J. Yamamoto, and H. Yokoyama, Phys. Rev. Lett. **92**, 185501 (2004), URL http://link.aps.org/doi/10.1103/PhysRevLett.92.185501.

[32] I. I. Smalyukh, O. D. Lavrentovich, A. N. Kuzmin, A. V. Kachynski, and P. N. Prasad, Phys. Rev. Lett. **95**, 157801 (2005).

[33] U. M. Ognysta, A. B. Nych, V. A. Uzunova, V. M. Pergamenschik, V. G. Nazarenko, M. Škarabot, and I. Muševič, Phys. Rev. E **83**, 041709 (2011), URL https://link.aps.org/doi/10.1103/PhysRevE.83.041709.

[34] S. Changizrezaei and C. Denniston, Phys. Rev. E **95**, 052703 (2017), URL https://link.aps.org/doi/10.1103/PhysRevE.95.052703.

[35] M. Ravnik, G. P. Alexander, J. M. Yeomans, and S. umer, Proceedings of the National Academy of Sciences **108**, 5188 (2011), http://www.pnas.org/content/108/13/5188.full.pdf, URL http://www.pnas.org/content/108/13/5188.abstract.

[36] T. A. Wood, J. S. Lintuvuori, A. B. Schofield, D. Marenduzzo, and W. C. K. Poon, Science **334**, 79 (2011), ISSN 0036-8075, http://science.sciencemag.org/content/334/6052/79.full.pdf, URL http://science.sciencemag.org/content/334/6052/79.

[37] K. Stratford, O. Henrich, J. S. Lintuvuori, M. E. Cates, and D. Marenduzzo, NATURE COMMUNICATIONS **5**, 3954 (2014).

[38] V. S. R. Jampani, M. Škarabot, S. Čopar, S. Žumer, and I. Muševič, Phys. Rev. Lett. **110**, 177801 (2013), URL https://link.aps.org/doi/10.1103/PhysRevLett.110.177801.

[39] R. P. Trivedi, M. Tasinkevych, and I. I. Smalyukh, Phys. Rev. E **94**, 062703 (2016), URL https://link.aps.org/doi/10.1103/PhysRevE.94.062703.

[40] I. Musevic and M. Skarabot, Soft Matter **4**, 195 (2008), URL http://dx.doi.org/10.1039/B714250A.

[41] D. F. Gardner, J. S. Evans, and I. I. Smalyukh, Molecular Crystals and Liquid Crystals **545**, 3/[1227] (2011), http://dx.doi.org/10.1080/15421406.2011.571966, URL http://dx.doi.org/10.1080/15421406.2011.571966.

[42] A. Antipova and C. Denniston, Phys. Rev. E **94**, 052704 (2016), URL https://link.aps.org/doi/10.1103/PhysRevE.94.052704.

[43] J. S. Lintuvuori, D. Marenduzzo, K. Stratford, and M. E. Cates, J. Mater. Chem. **20**, 10547 (2010).

[44] F. E. Mackay and C. Denniston, EPL (Europhysics Letters) **94**, 66003 (2011).

[45] F. E. Mackay and C. Denniston, Soft Matter **10**, 4430 (2014).

[46] P. G. de Gennes and J. Prost, *The Physics of Liquid Crystals* (Oxford University Press, 1993).

[47] A. N. Beris and B. J. Edwards, *Thermodynamics of Flowing Systems: with Internal Microstructure* (Oxford Engineering Science Series, 1994).

[48] C. Denniston, D. Marenduzzo, E. Orlandini, and J. M. Yeomans, Philosophical Transactions of the Royal Society of London A: Mathematical, Physical and Engineering Sciences **362**, 1745 (2004), URL http://rsta.royalsocietypublishing.org/content/362/1821/1745.

[49] C. Denniston, E. Orlandini, and J. M. Yeomans, Phys. Rev. E **63**, 056702 (2001), URL http://link.aps.org/doi/10.1103/PhysRevE.63.056702.

[50] C. Denniston, E. Orlandini, and J. M. Yeomans, EPL (Europhysics Letters) **52**, 481 (2000), URL http://stacks.iop.org/0295-5075/52/i=4/a=481.

[51] S. Plimpton, Journal of Computational Physics **117**, 1 (1995), ISSN 0021-9991, URL http://www.sciencedirect.com/science/article/pii/S002199918571039X.

[52] F. Mackay, S. Ollila, and C. Denniston, Computer Physics Communications **184**, 2021 (2013), ISSN 0010-4655.

[53] F. Mackay and C. Denniston, Journal of Computational Physics **237**, 289 (2013), ISSN 0021-9991.

[54] F. E. Mackay and C. Denniston, Soft Matter **9**, 5285 (2013).

[55] A. Antipova and C. Denniston, Soft Matter **12**, 1279 (2016).

[56] A. Antipova and C. Denniston, Phys. Rev. E **94**, 052704 (2016), URL https://link.aps.org/doi/10.1103/PhysRevE.94.052704.

[57] B. Frisken, Ph.D. thesis, University of British Columbia (1989).